Article Type: Full Paper

Plasma Polymerisation Using Helium Atmospheric-Pressure Plasma Jet with Heptylamine Monomer

Kyle G. Doherty, Jun-Seok Oh[#], Paul Unsworth, Carl M. Sheridan, Peter Weightman, James W. Bradley and Rachel L. Williams*

_____

Dr. K. G. Doherty

Department of Eye and Vision Science, University of Liverpool, Liverpool, L7 8TX, UK

Dr. J.-S. Oh

Department of Electrical Engineering and Electronics, University of Liverpool, Liverpool, L69 3GJ, UK

Dr. P. Unsworth,

Department of Physics, University of Liverpool, Liverpool, L69 3BX, UK

Dr. C. M. Sheridan,

Department of Eye and Vision Science, University of Liverpool, Liverpool, L7 8TX, UK

Prof. P. Weightman

Department of Physics, University of Liverpool, Liverpool, L69 3BX, UK

Prof. J. W. Bradley

Department of Electrical Engineering and Electronics, University of Liverpool, Liverpool, L69 3GJ, UK

Prof. R. L. Williams

Department of Eye and Vision Science, University of Liverpool, Liverpool, L7 8TX, UK, rlw@liverpool.ac.uk

[#] Current address is Graduate School of Engineering, Osaka City University, Osaka, 558-8585 Japan

Summary

Atmospheric-pressure plasma jets can be used to modify surfaces in a spatially-defined manner. Operating these jets in air is an efficient surface modification tool, however the resulting surface chemistries are limited by the plasma gases. In this study we demonstrate that plasma polymerisation with heptylamine on polystyrene surfaces, using an atmospheric pressure plasma jet, can enable mammalian cell attachment and growth. Importantly, the addition of the heptylamine monomer, in a helium carrier-gas, altered the spatially-defined treatment area in comparison to treatment with a helium plasma alone.

1 Introduction

Interest in the use of atmospheric pressure plasma jets (APPJs) as a method of surface functionalisation has continued to grow over recent years.[1-7] Much of the work focuses on operating in air, which enables processing to be conducted more cost effectively than in systems requiring a vacuum chamber. There are many possible applications for APPJs including plasma medicine, anti-fouling coatings and modification of biomaterials to tune cellular response. We have demonstrated that polystyrene surface functionalisation, using a helium jet operated through a micro-APPJ with 100-µm internal diameter, enabled lens epithelial cell growth in a spatially-defined manner.[2] Spatially-resolved plasma treatment could allow the efficient creation of chemically heterogeneous surfaces. Lately other researchers have also been focusing on the potential to produce spatially resolved surface functionality using plasma jet treatment.[8-12] Motrescu and Masaaki created amine functionalities of 2-3 µm diameter, by the addition of ammonia to a He primary gas feed.[11] Further information regarding localised treatment can be found in the recent review by Fanelli and Fracassi.[13] However, to our knowledge the effects of the addition of monomers to an APPJ's spatial resolution has not been previously studied.

The use of inert gases results in incorporation of oxygen from the air surrounding the plasma onto the treated surfaces. The use of APPJs for plasma polymerisation, however, offers the possibility to create surfaces modified with a variety of functional groups, depending on the monomer added to the APPJ discharge. Over 10 years ago Benedikt et al. demonstrated the deposition of carbon[14] and siloxane[15] surfaces using APPJs. More recently, researchers have incorporated many different monomers into APPJs operated in air including: hexafluorobezene,[16] acrylic acid,[17] acetylene,[18] organosilanes,[19] hexamethyldisilazane,[20, 21] Fewer APPJ plasma polymerised monomers have been studied for their effects on cellular

attachment. Polyethylene glycol, poly ε-caprolactone and acrylic acid have been deposited on various substrates to either promote or inhibit cellular attachment.[17, 22-27]

We aimed to demonstrate that plasma polymerisation of heptylamine using an APPJ in air[28] can incorporate nitrogen species onto a polymer surface and that these surfaces can be used to direct cell growth. We also studied the effects of heptylamine monomer addition on the spatial resolution of the treatment. In this study polystyrene (PS) was used as a model polymer surface as its hydrocarbon chemistry enables easy observation of expected changes and it does not normal support cell growth without plasma treatment. The study aimed to demonstrate the potential of APPJ plasma polymerisation to modify the surfaces of intraocular lenses (IOL). IOLs are implanted after cataract surgery to restore vision, however they suffer from a secondary complication associated with scarring. This scarring response has been associated with the interaction between the lens tissues and cells with the IOL materials.[29] It was hypothesised that spatially resolved surface functionalisation with specific chemical groups could influence the attachment and migration of lens epithelial cells across the IOL and, therefore, APPJ plasma-polymerisation may be a cost-effective method of lens surface modification.

2 Experimental Section

2.1 APPJ Configuration

The APPJ setup for monomer mixing has previously been described by Oh and Bradley (2013).[28] The APPJ consisted of a quartz capillary with a single powered electrode was approximately 40 mm back from the capillary nozzle. The electrode was excited by a sinusoidal voltage (8 kV_{p-p}) at fixed frequency of 10 kHz. Helium flowed into the primary capillary at a rate of 500 sccm. Helium was bubbled through heptylamine in a round bottom flask at room

temperature at 20-100 sccm and the helium: heptylamine precursor was introduced into the main plasma downstream via the secondary capillary, approximately 25 mm upstream from the nozzle (**Figure 1**).

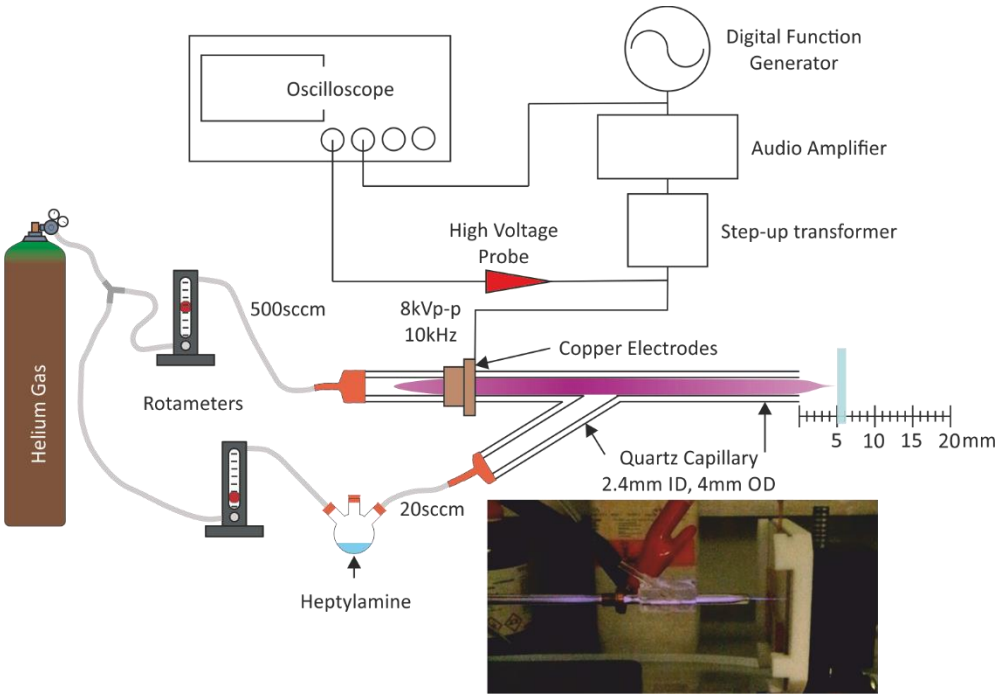

Figure 1 Schematic of APPJ setup, with photograph inset.

2.2 Substrate Preparation

PS was prepared as previously described.[2] Briefly, a PS sheet of thickness 1.2 mm (Goodfellow Cambridge Ltd.) was cut into squares approximately 10 mm × 10 mm. Samples were ultrasonicated in isopropanol for 180 s, dried under N_2 flow and allowed to relax under atmosphere for a day before use. Samples were treated approximately in the centre. PS was placed 5 mm from the nozzle and treated for 10 minutes with helium alone (HE-PS) or plasma polymerised heptylamine (ppHEPTYL-HE-PS). Untreated PS (UT-PS) served as a control.

2.3 X-ray Photoelectron Spectroscopy (XPS)

The instrument used for these studies has been described previously.[30] It was constructed by VSW ltd. of Manchester, UK. The instrument is fitted with a multicrystal Al K X-ray monochromator on a 0.7-m Rowland circle which subtends a solid angle of ~0.1 sterradian at the specimen thus providing high sensitivity XPS capability at 1486.6 eV. The x-ray 'spot' focused on a sample surface has a size of ~1.5 × 7 mm. Charge compensation was provided by an electron flood gun. Broad scan spectra were acquired at pass energies of 100 eV at a spatial resolution of 1 mm. The O1s/C1s and N1s/C1s ratios were calculated from the peak intensities in the broad scan spectra.

2.4 Contact Angle Measurements

The drop shape analysis system (DSA100m, Krüss) was used to measure contact angles using the sessile drop method. Droplets of water were dispensed across the surface with a lateral resolution of 500 μm, images of the droplets were captured and analysed using the circle method, which can be calculated using by equation 1

$$\tan(\theta/2) = h/r \qquad (1)$$

where *h* is the drop height and *r* (=*L*/2) is the radius of the droplet base (DSA3 software, Krüss). Contact angle measurements were taken across the centre of samples to determine the diameter of the treatment area. Four samples were used for each treatment parameter.

2.5 Atomic Force Microscopy (AFM) Analysis

AFM was used to investigate the effect APPJ treatment had on surface topography. A Multimode 8 AFM with Nanoscope V controller (Bruker) was used in normal tapping mode with a silicon cantilever of spring constant 40 N m^{-1}. A 500 nm^2 region was scanned at a rate of 1 Hz with 512 samples / line. The scans were subjected to 0^{th} order plane fit, to remove

image bow, and 0^{th} and 1^{st} order flattening, to centre data and remove tilt. The mean root mean square roughness (R_q) for each treatment were averaged from 4 scans in the centre of the samples. Four replicates were used for each treatment, except for HE-PS, of which there were three.

2.6 Cell Culture

For cell culture, a human LEC line (B3)[31] was used (kindly donated by Prof. Barbara Pierscoinek of Nottingham Trent University, UK). Cells were maintained at 37 °C and 5 % CO_2 in Eagles Minimum Essential Media (Sigma) supplemented with 10 % (v/v) foetal calf serum (Sigma) and 2 mM L-glutamine (Sigma). The cell media was replaced every 3-4 days. Passaging and cell seeding was conducted by enzymatic digestion using 0.5 mg ml^{-1} trypsin and 0.2 mg ml^{-1} EDTA (Sigma) in phosphate buffered saline (PBS) solution (Oxoid). Cells seeded at a density of 1×10^4 cells cm^{-2} onto the samples. Prior to cell seeding on treated and untreated PS, samples were sterilised by UV treatment using CL-1000 crosslinker (UVP) for 5 minutes at 150 mJ cm^{-2}. Cells were seeded onto four samples for each treatment and for UT-PS and tissue culture polystyrene (TCPS) control and the experiment was repeated twice.

2.7 Immunocytochemistry

Cells were grown on the substrates for 1, 4 and 7 days and were fixed and stained as previously described.[2] Briefly, cells were fixed in 10% neutral buffered formaldehyde for 10 minutes, permeabilised with 1 % triton X-100 solution (Sigma) for 5 minutes then stained with phalloidin and DAPI (4',6-Diamidino-2-Phenylindole, Dihydrochloride). Cells were imaged with an Axiovert 200 inverted fluorescent microscope (Zeiss), with 10× objective for cells counts and a 4× objective for image stitching. Nuclei were counted using ImageJ software. The 4× images were stitched together using MosiacJ plug-in for ImageJ[32] and the diameter of the

cell growth area was measured using AxioVision software v.4.8.1.0 (Zeiss). 3 or 4 samples were used for each parameter at each time point.

2.8 Statistical Analysis

Statistical analysis was done using SPSS v. 20 statistics software (SPSS, IBM) and results are reported as means ± standard deviation. Statistical significance was measured by one-way ANOVA followed by Tukey's test or Dunnett's T3 test if homogeneity of variances was upheld or violated, respectively. Statistical significance was assumed when $p<0.05$.

3 Results and Discussion

3.1 XPS Analysis

3.1.1 Surface Functionalities on the Modified PS Surface

Broad scan spectra were obtained for UT-PS, HE-PS and ppHEPTYL-HE-PS which had heptylamine flow rates of 20, 50 and 100 sccm. Broad scan spectra were resolved into 3 peaks: C1s, N1s and O1s. From the area beneath these peaks the total atomic concentration was determined. The broad scan spectra of UT-PS predominately contains a carbon C1s peak with trace amounts of oxygen and very little nitrogen (**Table 1**). A considerable O1s (23.2%) peak was also observed in the spectra for HE-PS, with minimal nitrogen present (0.8%). With the addition of 20 sccm heptylamine to the plasma the spectra clearly demonstrated a higher oxygen content (40.8%) compared to HE-PS (as seen from the O1s/C1s ratio, Table 1), also a substantial nitrogen peak was observed (13.9%). These were the highest concentrations of nitrogen and oxygen observed for all samples. The presence of both nitrogen and oxygen were observed with the addition 50 sccm and 100 sccm heptylamine to the plasma flow, however the relative peak intensities were smaller than those observed on the 20 sccm parameter (Table 1).

We observed decreased APPJ stability at higher monomer flow rates (50 & 100 sccm). This may be why the lowest monomer flow rate (20sccm) was the most efficient at nitrogen functionalisation. However, Oh et al. observed the highest concentrations of positive ionic heptylamine oligomers in the plasma jet effluent at medium flow rates 40-60 sccm. Only the positive ionic oligomers were studied so perhaps negatively charged ionic oligomers, or even neutral species, play a more dominant role in surface polymerisation at lower flow rates.[28] The increased concentration of oxygen on ppHEPTYL-HE-PS compared to HE-PS is possibly due to deposition of a plasma polymerised thin film creating a thicker oxygen-containing coating.

3.1.2 Spatial Distribution Nitrogen and Oxygen on the Treated Surface

XPS broad scans were also obtained across sample surfaces with a spatial resolution of 1 mm. Almost no nitrogen was observed at any position on UT-PS (**Figure 2a**). The surface concentration of nitrogen on 20 sccm ppHEPTYL-HE-PS was >10% at all positions and reached a maximum of 14.6%. The maximum nitrogen concentration on 50 sccm ppHEPTYL-HE-PS was 12.6%: this decreased with distance from the centre to a minimum of 2.3% at the edge. The spectra for 100 sccm ppHEPTYL-HE-PS was similar to the 50 sccm sample, with a maximum nitrogen concentration of 10.7% in the centre decreasing to <1% at the edge of the sample.

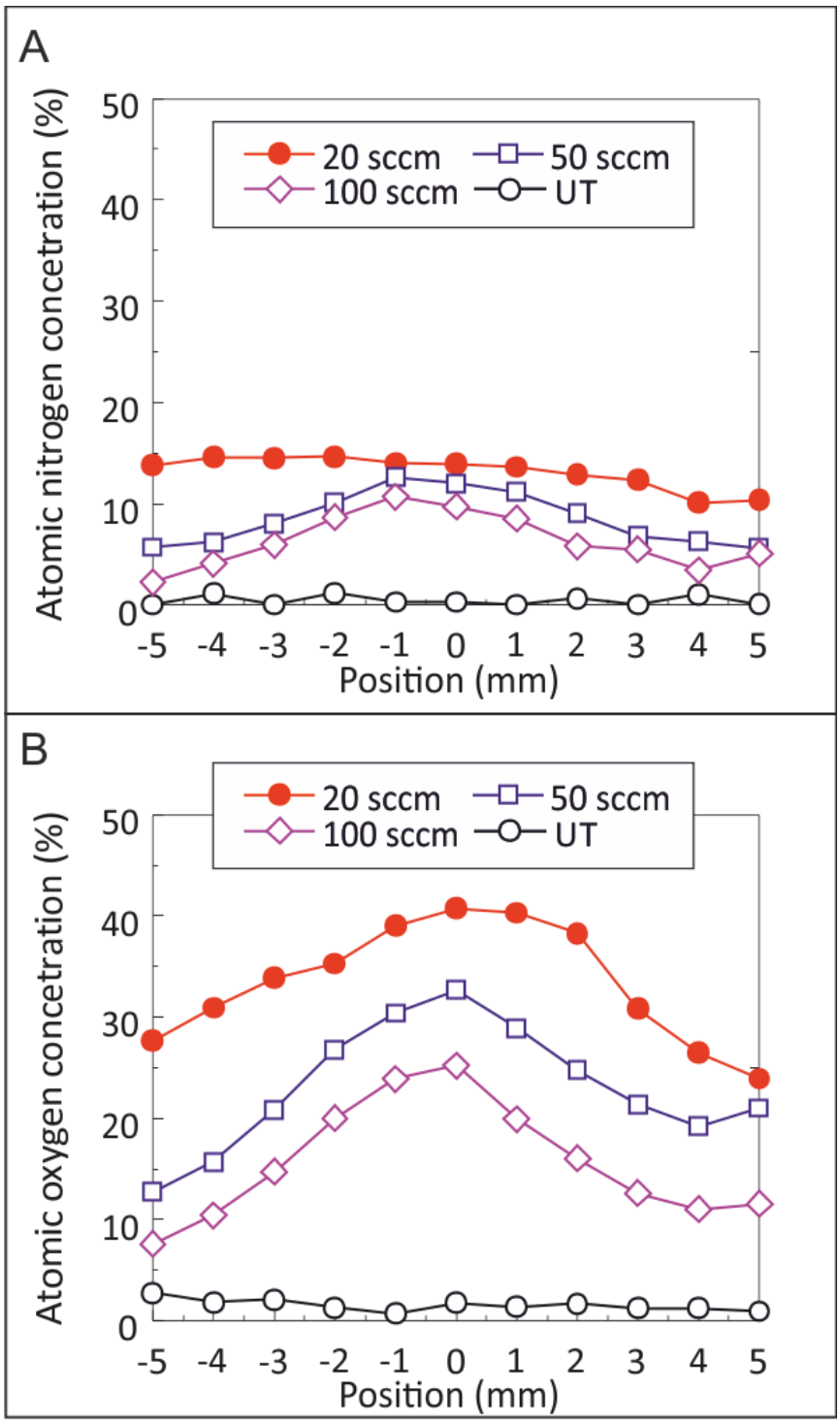

Figure 2 Line graph of the atomic A) nitrogen and B) oxygen concentrations, as determined from x-ray photoelectron spectroscopy broad scan spectra (100 eV pass energy), across the surface of untreated polystyrene (UT-PS) and polystyrene treated with a mixture of 500 sccm helium and 20sccm heptylamine, 50 sccm heptylamine and 100 sccm heptylamine. Spectra were taken with a spatial resolution of 1 mm. Single samples were used.

Very little surface oxygen concentration was observed at any position on UT-PS (≤2.3%) (Figure 3b). The oxygen concentration on all the various ppHEPTYL-HE-PS samples decreased with distance from the centre. The oxygen concentration at each point decreased with an increasing flow rate. These data demonstrate the entire surface of samples were treated and the extent of treatment, i.e. the concentration of nitrogen and oxygen, decreases with an increase in heptylamine flow rate.

3.2 Contact Angle Analysis

3.2.1 CA Profiles

The average CA of UT-PS was 77.2 ± 3.9° (**Figure 3A**), which was similar to our previous work.[2, 33] The entire 10 × 10 mm^2 sample surface of HE-PS was treated. The CA ranged from 20.3° in the centre to ≈31 ° at the edges. The CAs of HE-PS and ppHEPTYL-HE-PS were significantly lower ($p<0.001$) than UT-PS at all positions. A greater change in CA across the surface was observed for ppHEPTYL-HE-PS compared to HE-PS or UT-PS samples; it was >40 ° at the edges and <20 ° in the centre.

The CA of ppHEPTYL-HE-PS was significantly higher ($p<0.05$) than HE-PS at the 4 mm-3 mm positions at each side. ppHEPTYL-HE-PS had a significantly lower ($p<0.05$) CA at the 2 mm-0.5 mm positions (total 1.5 mm) right of the centre: this demonstrates that treatment with the addition of heptylamine monomer created a different spatial resolution compared to treatment with helium plasma alone, which is evident in 2D contact angle maps (Figure 3B). This change in spatial modification is an important consideration when attempting to design systems for spatially resolved treatment.

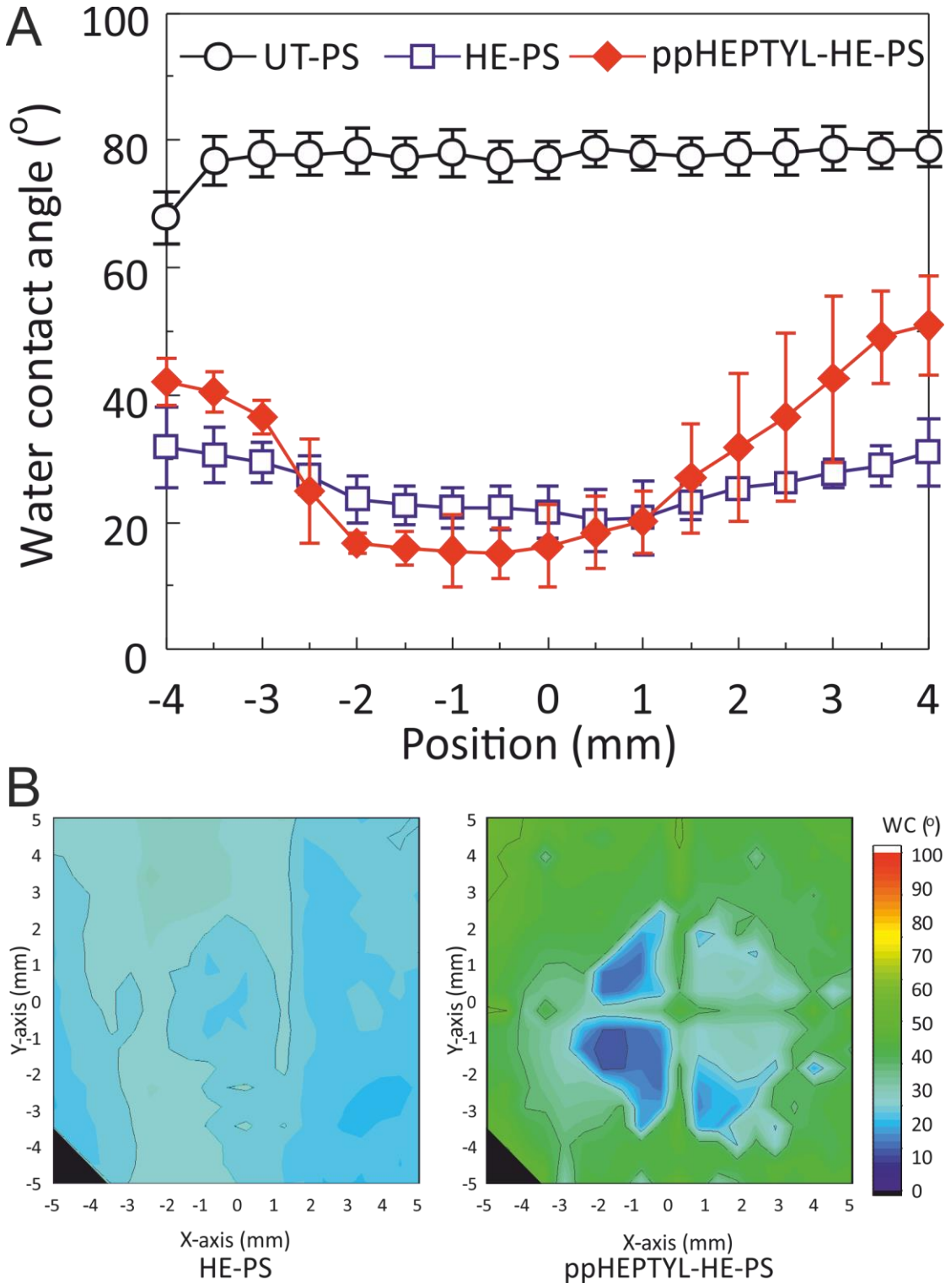

Figure 3 A) Line graph of contact angle profiles taken across UT-PS and HE-PS or ppHEPTYL-HE-PS. B) 2-D CA plots of HE-PS and ppHEPTYL-HE-PS. Contact angle resolution 0.5 mm.

HE-PS had a more uniform surface functionalisation compared to the ppHEPTYL-HE-PS. The spatially defined treatment on ppHEPTYL-HE-PS observed in XPS (Figure 3) and CA (Figure 4) may have been due to decreased spreading of monomer fragments because of their mass, or increased polymerisation on the surface under the focus of the jet. In our previous work we observed relatively large treatment areas for small APPJ nozzle diameters. We hypothesised that this was due to the gaseous transport of excited secondary radicals along the material surface perpendicular to the jet outflow. [2, 34, 35] Other work has also demonstrated the spreading of APPJ gas outflows when they strike a surface.[36-39] However, to our knowledge no work has been conducted to observe APPJ outflow, using Schlieren photography, with the addition of monomer precursor containing gas flow. As the flow rate of these precursors are typically very low it is unlikely changes would be observable, however it is possible that excited molecules with higher masses may not travel as far from the focus of the APPJ outflow.

3.3 AFM

The squared roughness (Rq) of UT-PS = 0.6 ± 0.4 nm (**Figure 4**) and was not significantly different to either HE-PS or ppHEPTYL-HE-PS ($p>0.5$). HE-PS had the greatest roughness (Rq=0.8 ± 0.2 nm) compared to UT-PS and ppHEPTYL-HE-PS. HE-PS had a significantly higher roughness than ppHEPTYL-HE-PS (Rq=04 ± 0.2 nm; $p<0.001$).

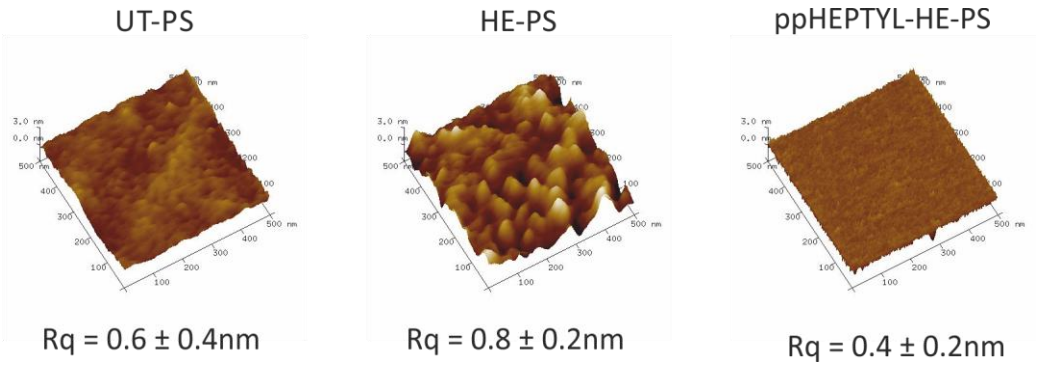

Figure 4 AFM micrographs including root mean squared roughness (Rq) values of UT-PS, HE-PS and ppHEPTYL-HE-PS.

The topography of the HE-PS appears similar to that treated with a helium microplasma jet in our previous work, which is likely a result of ionic etching.[2] However, the ppHEPTYL-HE-PS has a much smoother surface suggesting deposition of a thin film.[40]

3.4 Cell Culture

3.4.1 Spatial Control of Cell Growth

Surface characterisation has demonstrated the hetrogenous incorporation of nitrogen and oxygen functionality on ppHEPTYL-HE-PS. Cells were grown on materials for up to 7 days, and the number of cells in the centre and at discrete positions (1.5 mm, 3 mm and 4 mm) from the centre were counted, to evaluate the cellular response to surface treatment. Diameter of confluent cell growth area was determined from stitched images taken with a 4× objective taken across the samples.

At day 7 there were 512-795 cells per field of view across all positions of tissue culture polystyrene (TCPS) control (**Figure 5**). There were almost no cells at any position on UT-PS (~1 cell per field of view) and there were significantly fewer cells than TCPS at every position ($p<0.001$).

On HE-PS there were 1065 ± 250 cells per field of view in the centre position, which was more than any other material at this position. The number of cells decreased from the centre to 4 mm position; the pattern of cell growth was similar on days 1 and 4 (data not shown). Cells first became confluent in the centre and this confluent area spread (Figure 5B). However UT-PS had significantly fewer cells at every position compared to HE-PS ($p<0.001$), therefore the entire sample surface was functionalised to support cell culture and this was likely due to

surface functionalisation by excited particles spread across the whole surface due to the gas flow. [2, 34-38] This result was expected; in our previous work we obtained treatment areas with a diameter of 4.5 mm, from a 100 µm ID nozzle, after only 20 s of treatment with a helium APPJ.[2] Treatment area also increases as the distance between the sample and the nozzle increases.[41] Only scattered cells were present at the periphery of the sample (Figure 5C).

On ppHEPTYL-HE-PS there were 472 ± 397 cells per field of view in the centre position, which decreased to 14 ± 19 cells per field of view at the 4 mm position. This corresponded closely to the changes observed in the contact angle data (Figure 3). Although the difference between UT-PS and ppHEPTYL-HE-PS at the 4 mm position was only 13 cells per field of view, this was significantly different ($p=0.004$), therefore ppHEPTYL-HE-PS could not be considered untreated at any position following 7 days of culture. However, ppHEPTYL-HE-PS did display a more confined treatment region compared to HE-PS (Figure 5B and 5C). Areas of confluent cell growth were similar on both HE-PS and ppHEPTYL-HE-PS at day 1 (Figure 5B). The cell growth area expanded more rapidly on HE-PS as the entire sample surface was relatively hydrophilic compared to ppHEPTYL-HE-PS (Figure 3B), which maintained a defined growth boundary (Figure 5C). Posterior capsule opacification (PCO) is the secondary scarring complication which occurs following implantation of a polymeric intraocular lens. In PCO LECs migrate from the anterior side of the lens capsule to the previously cell free posterior, where they dedifferentiate into fibroblast-like cells which cause scarring. If LEC migration to the posterior can be inhibited, or if the LECs can be maintained in their epithelial phenotype once at the posterior of the implanted lens, the incidence PCO could be reduced or eliminated. We have demonstrated that APPJ plasma polymerisation creates a central treated region, which encourages LEC growth, surrounded by a region of growth inhibition. It is important to note these different patterns of cell growth and contact angle at the periphery of treated surfaces,

despite what was likely a small increase in flow rate at the nozzle on the addition of heptylamine. This may suggest that addition of monomers affects the spatial resolution of treatment by altering the reactions within the plasma.

Cells interact with surfaces via adsorbed proteins that are either present in the culture media and/or secreted by the cells.[42] Thermodynamic interactions between the amino acids within proteins and the chemical structure of surfaces determine the confirmation of the proteins when they adsorb onto the surfaces. It is well documented that creating a more hydrophilic polystyrene surface, by the addition of oxygen and/or nitrogen, will cause the adsorption of proteins in a conformation expressing specific amino acid sequences which increase cellular attachment.[42-47] Work by Underwood et al. clearly demonstrated this using the binding of fibronectin to UT-PS and TCPS (which is hydrophilic). They observed that although there was more fibronectin on UT-PS, the arginine-glycine-aspartic acid (RGD) peptide responsible for cell attachment was only detected via antibody staining when fibronectin was bound to TCPS.[47] Surface topography can also have a strong influence on cellular behaviour.[48] However, in our work both HE-PS and ppHEPTYL-HE-PS, the most rough and smoothest surfaces respectively, supported LEC growth, suggesting that it was the addition of oxygen and nitrogen (Table 1) that encouraged protein adsorption in a conformation that enables LEC attachment and growth.

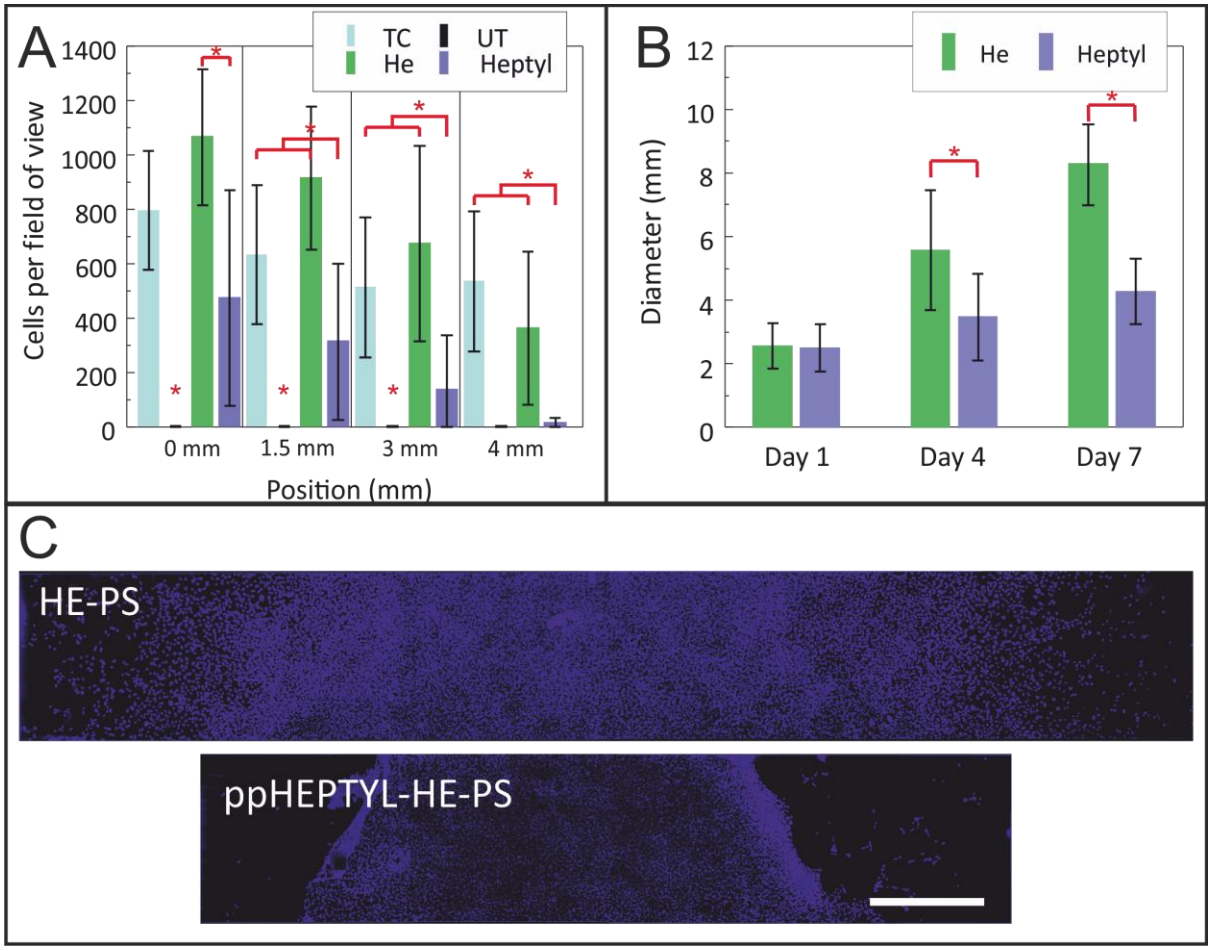

Figure 5 A) Bar chart displaying mean number of DAPI stained B3 human lens epithelial cells (LECs) per field of view at the centre of samples and 1.5 mm, 3 mm and 4 mm from the centre of samples at day 7. Significant differences are only graphically displayed for intra-parameter differences. B) Bar chart of diameters of cell growth across samples measured from stitched. C) Representative stitched micrographs of fluorescently stained B3 LECs at day 7 on HE-PS and ppHEPTYL-HE-PS. * indicates significant difference of $p<0.05$.

3.4.3 Cell Morphology

Cells on all hydrophilic materials (TCPS, HE-PS and ppHEPTYL-HE-PS) displayed actin stress fibres, which is a fibrotic morphology (**Figure 6**), despite having a more cuboidal appearance in phase contrast microscopy (data not shown). As the LECs used in this study are genetically transformed to continuously replicate [31] they can continue to proliferate when

confluence has been reached: this likely accounts for the overlapping actin staining and stress fibres present, which is clearly evident from the very confluent HE-PS samples (figure 6).

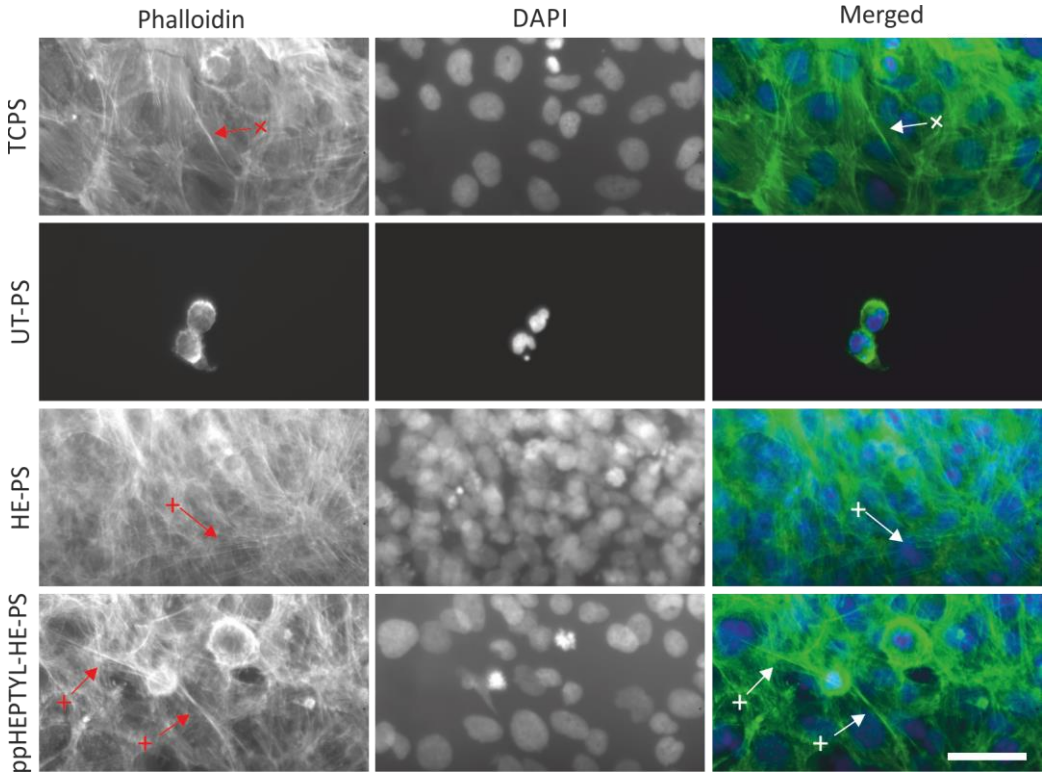

Figure 6 Representative high magnification micrographs of human B3 lens epithelial cells (LECs) with phalloidin f-actin staining (green), DAPI nuclear staining (blue) and merged images taken on TCPS, UT-PS, helium treated PS, and heptylamine treated PS at day 7. + = actin stress fibres. Scale bar = 50 µm.

Although the presence of stress fibres may indicate a change in morphology of LECs this paper demonstrates a proof of principle that the addition of monomers to APPJ operated in air can be used to add chemical functional groups to polymer surfaces, which can influence cell-surface interactions. In this work we used PS as a model polymer substrate, because its hydrocarbon structure would easily demonstrate the hypothesised addition of oxygen and nitrogen by XPS analyses, and the subsequent change in wettability from UT-PS hydrophobic character. The majority of modern IOLs are made from acrylic or silicone-based materials; the oxygen content

in these made analyses more complicated at this exploratory stage, particularly at the sample periphery. Due to the mechanisms of plasma polymerisation it is expected that this process would produce similar surfaces on other polymers. The B3 LEC line was used as a convenient model to examine the effect of treatment on cell attachment. Although the HE-PS, and to a lesser extent ppHEPTYL-HE-PS, induced stress fibres indicative of fibrosis, we have demonstrated that the process of plasma polymerisation with an APPJ can created spatially-defined treatment with chemical functionalities that will be tailorable with the addition of different monomers.

4 Conclusions

We have demonstrated that plasma polymerisation of heptylamine in ambient air with an APPJ can incorporate nitrogen species onto a polymer surface. Incorporation of heptylamine precursor into the plasma stream created a more refined treatment area in the centre of the sample, which highlights the effect that monomer addition has on APPJ treatment area. The surfaces treated with heptylamine APPJ supported the growth of human LEC cell line. This demonstrates the potential to use an APPJ system to create plasma polymerised surfaces to promote the attachment and growth of a functional LEC monolayer.

Acknowledgements: The authors would like to acknowledge the Engineering and Physical Sciences Research Council (EPSRC) for supporting this work on grant references: EP/G048444/1 & EP/M002209/1. All data relating to this research is openly available from Liverpool Research Data Catalogue at *http://dx.doi.org/10.17638/datacat.liverpool.ac.uk/569*. The authors would like to thank Mr. A. Roby at University of Liverpool, for much help with the plasma jet system. The authors are grateful to School of Engineering (University of

Liverpool) for access to the AFM, and to Drs. Tim Joyce and Riaz Akhtar for providing technical assistance.

Keywords: atmospheric-pressure plasma jet, cell adhesion, plasma polymerization, polystyrene (PS), water contact-angle (WCA)

[1] E. J. Szili, A. S. Al-Baraineh, P. M. Bryant, R. D. Short, J. W. Bradley, and D. A. Steele, *Plasma Process. Polym.*, **2011**. *8,* 1;
[2] K. G. Doherty, J.-S. Oh, P. Unsworth, A. Bowfield, C. M. Sheridan, P. Weightman, J. W. Bradley, and R. L. Williams, *Plasma Process. Polym.*, **2013**. *10,* 11;
[3] M. Nagatsu, M. Kimpara, R. Hu, and T. Abuzairi, *J. Photopolym. Sci. Tech.*, **2017**. *30,* 3;
[4] A. Sarani, N. De Geyter, A. Y. Nikiforov, R. Morent, C. Leys, J. Hubert, and F. Reniers, *Surf. Coat. Technol.*, **2012**. *206,* 8;
[5] A. Van Deynse, P. Cools, C. Leys, R. Morent, and N. De Geyter, *Surf. Coat. Technol.*, **2015**. *276,*
[6] S. David, W. Andrew, B. Jerome, and W. Erik, *Plasma Sources Sci. Technol.*, **2016**. *25,* 6;
[7] J.-S. Oh, O. T. Olabanji, C. Hale, R. Mariani, K. Kontis, and J. W. Bradley, *J. Phys. D: Appl. Phys.*, **2011**. *44,* 15;
[8] Ö. Birer, *Appl. Surf. Sci.*, **2015**. *354,* Part B;
[9] T. Wang, B. Yang, X. Chen, X. Wang, C. Yang, and J. Liu, *Appl. Surf. Sci.*, **2016**. *383,*
[10] D. F. Williams, E. J. C. Kellar, D. A. Jesson, and J. F. Watts, *Appl. Surf. Sci.*, **2017**. *403,*
[11] I. Motrescu and M. Nagatsu, *ACS Appl. Mater. Interfaces*, **2016**. *8,* 19;
[12] P. Bosso, F. Fanelli, and F. Fracassi, *Plasma Process. Polym.*, **2016**. *13,* 2;
[13] F. Fanelli and F. Fracassi, *Surf. Coat. Technol.*, **2017**. *322,*
[14] J. Benedikt, K. Focke, A. Yanguas-Gil, and A. Von Keudell, *Appl. Phys. Lett.*, **2006**. *89,* 25;
[15] J. Benedikt, V. Raballand, A. Yanguas-Gil, K. Focke, and A. Von Keudell, *Plasma Phys. Controlled Fusion*, **2007**. *49,* 12b;
[16] C. Huang, C. H. Liu, W. T. Hsu, and T. H. Chou, *J Non Cryst. Solids.*, **2010**. *356,* 35-36;
[17] O. Carton, D. Ben Salem, S. Bhatt, J. Pulpytel, and F. Arefi-Khonsari, *Plasma Process. Polym.*, **2012**. *9,* 10;
[18] A. H. Ricci Castro, F. V. P. Kodaira, V. Prysiazhnyi, R. P. Mota, and K. G. Kostov, *Surf. Coat. Technol.*, **2017**. *312,*
[19] P. Bringmann, O. Rohr, F. J. Gammel, and I. Jansen, *Plasma Process. Polym.*, **2009**. *6,* 1;
[20] F. V. P. Kodaira, A. H. Ricci Castro, V. Prysiazhnyi, R. P. Mota, A. Quade, and K. G. Kostov, *Surf. Coat. Technol.*, **2017**. *312,*
[21] F. Mussano, T. Genova, E. Verga Falzacappa, P. Scopece, L. Munaron, P. Rivolo, P. Mandracci, A. Benedetti, S. Carossa, and A. Patelli, *Appl. Surf. Sci.*, **2017**. *409,*

[22] S. Bhatt, J. Pulpytel, S. Mori, M. Mirshahi, and F. Arefi-Khonsari, *Plasma Process. Polym.*, **2014**. *11*, 1;
[23] M. Gozutok, A. Baitukha, F. Arefi-Khonsari, and H. T. Sasmazel, *J. Phys. D: Appl. Phys.*, **2016**. *49*, 47;
[24] Y. Mengmeng, H. Jun, Y. Jinsong, C. Guangliang, and Q. Shanqing, *Materials Research Express*, **2017**. *4*, 7;
[25] B. Nisol, A. Meunier, C. Buess-Herman, and F. Reniers, *Plasma Process. Polym.*, **2015**. *12*, 9;
[26] B. Nisol, G. Oldenhove, N. Preyat, D. Monteyne, M. Moser, D. Perez-Morga, and F. Reniers, *Surf. Coat. Technol.*, **2014**. *252*,
[27] K. N. Pandiyaraj, A. Arun Kumar, M. C. Ramkumar, P. V. A. Padmanabhan, A. M. Trimukhe, R. R. Deshmukh, P. Cools, R. Morent, N. De Geyter, V. Kumar, P. Gopinath, and S. K. Jaganathan, *J. Phys. Chem. Solids*, **2018**. *123*,
[28] J.-S. Oh and J. W. Bradley, *Plasma Process. Polym.*, **2013**. *10*, 10;
[29] S. Saika, *Prog. Retin. Eye Res.*, **2004**. *23*, 3;
[30] P. Weightman, *Phys. Scr.*, **1992**. *T41*,
[31] U. P. Andley, J. S. Rhim, J. L. T. Chylack, and T. P. Fleming, *Invest. Ophthalmol. Vis. Sci.*, **1994**. *35*, 7;
[32] P. Thévenaz and M. Unser, *Microsc. Res. Tech.*, **2007**. *70*, 2;
[33] K. Doherty, J. S. Oh, C. Sheridan, R. Williams, and J. W. Bradley, presented at 24th European Conference on Biomaterials, ESB 2011, Dublin, **2011**
[34] J.-S. Oh, Y. Aranda-Gonzalvo, and J. W. Bradley, *J. Phys. D: Appl. Phys.*, **2011**. *44*, 36;
[35] J. W. Bradley, J. S. Oh, O. T. Olabanji, C. Hale, R. Mariani, and K. Kontis, *IEEE Trans. Plasma Sci.*, **2011**. *39*, 11 PART 1;
[36] Y. Zheng, L. Wang, W. Ning, and S. Jia, *J. Appl. Phys.*, **2016**. *119*, 12;
[37] E. Robert, T. Darny, S. Dozias, S. Iseni, and J. M. Pouvesle, *Physics of Plasmas*, **2015**. *22*, 12;
[38] M. Boselli, V. Colombo, E. Ghedini, M. Gherardi, R. Laurita, A. Liguori, P. Sanibondi, and A. Stancampiano, *Plasma Chem. Plasma Process.*, **2014**. *34*, 4;
[39] D. Liu, T. He, Z. Liu, S. Wang, Z. Liu, M. Rong, and M. G. Kong, *Plasma Process. Polym.*, **2018**. *15*, 10;
[40] S. Hwang, H. Seo, D.-C. Jeong, L. Wen, J. G. Han, C. Song, and Y. Kim, *Sci. Rep.*, **2015**. *5*,
[41] E. J. Szili, S. A. Al-Bataineh, P. M. Bryant, R. D. Short, J. W. Bradley, and D. A. Steele, *Plasma Process. Polym.*, **2011**. *8*, 1;
[42] *Biomaterials Science: An Introduction to Materials in Medicine*, B. D. Ratner, A. S. Hoffman, F. J. Schoen, and J. E. Lemons Eds., Elsevier Academic Press, London **2004**
[43] R. A. D'sa, G. A. Burke, and B. J. Meenan, *Acta Biomater.*, **2010**. *6*, 7;
[44] A. Sethuraman, M. Han, R. S. Kane, and G. Belfort, *Langmuir*, **2004**. *20*, 18;
[45] R. A. D'sa, G. A. Burke, and B. J. Meenan, *J. Mater. Sci. Mater. Med.*, **2010**. *21*, 5;
[46] F. Grinnell and M. K. Feld, *J. Biol. Chem.*, **1982**. *257*, 9;
[47] P. A. Underwood, J. G. Steele, and B. A. Dalton, *J. Cell Sci.*, **1993**. *104*, 3;
[48] M. Macgregor-Ramiasa, I. Hopp, A. Bachhuka, P. Murray, and K. Vasilev, *Acta Biomater.*, **2017**. *56*,

Table 1 Atomic concentrations as percentages of carbon, nitrogen and oxygen for untreated PS (UT-PS), polystyrene treated for 10mins with helium (He), polystyrene treated with a mixture of helium and 20 sccm heptylamine (20 sccm), 50 sccm heptylamine (50 sccm) and 100 sccm heptylamine (100 sccm). Total concentration was derived from the area of peaks in broad scan spectra taken in the centre of samples (100 eV pass energy). Single samples were used.

		UT-PS	He	20 sccm	50 sccm	100 sccm
Atomic concentration (%)	C1s	97.9	76.1	45.4	63.1	65.4
	N1s	0.3	0.8	13.9	10.1	10.7
	O1s	1.8	23.2	40.8	26.8	23.9
	O/C ratio	0.02	0.30	0.90	0.42	0.37
	N/C ratio	0.00	0.01	0.31	0.16	0.16

5 Graphical Abstract

To quickly and cheaply create spatially-defined chemical patterns on surfaces would be beneficial tool in many fields, including biomaterials, and may be achieved with plasma polymerisation using atmospheric-pressure plasma jets. The addition of heptylamine monomer in a helium plasma jet alters the surface chemistry, treatment pattern and cellular response compared to a helium plasma alone.